dimensional structure. A critical issue in creating photonic materials is how to fill the interstitial space completely with a component that has a high refractive index. We therefore electrodeposited group II–VI semiconductors into colloidal sediments, filling the interstitial space with materials of high refractive index (Fig. 1). The electrodeposited materials still allow the colloidal template to be removed, which is necessary to maximize the refractive-index contrast.

Electrodeposition should be an ideal way to fill topologically complex structures because it starts from deep within the structure and then grows out towards the exposed surfaces. We obtained microporous cadmium–selenium (CdSe) structures by potentiostatic[11] deposition in the interstitial space of a polystyrene colloidal template (Fig. 1a,b). Cadmium sulphide (CdS) was also grown by galvanostatic[12] (Fig. 1c) and potentiostatic (results not shown) deposition in colloidal assemblies, again yielding three-dimensionally periodic structures after the template is removed.

Because both CdS and CdSe have high refractive indices (2.5 at 600 nm and 2.75 at 750 nm, respectively), these structures can have deep gaps in their photonic band structure after the template is removed. CdS and CdSe are promising materials for photonic applications because, unlike most other high-refractive-index materials, they are optically transparent in the visible and near-infrared region of the spectrum.

One of the critical requirements for the existence of a true omnidirectional photonic band gap is three-dimensional periodicity and uniformity. Our template-directed electrodeposition of semiconductors results in three-dimensional structures (Fig. 1b,c), as indicated by the clearly visible holes into the layer below in all the systems. These holes form at contact points between the spheres of the template, and their arrangement on a triangular lattice is evidence that the hollow voids are on a hexagonal close-packed array.

As well as determining the three-dimensional structure, the holes between the voids allow for the complete removal of the template by solvent or acid, or through burnout. Our electrodeposited materials appear to be dense, as observed in high-magnification scanning electron micrographs of other template-directed electrodepositions[11]. As a result, the microporous structures shrink by only a tiny amount ($<2\%$) when the template is removed.

Template-directed electrodeposition is well suited to creating three-dimensional microstructures: many materials of high refractive index can be electrodeposited, including semiconductors of groups II–VI, III–V and IV, all of which are very reluctant to form three-dimensional microstructures by traditional techniques. These materials, which have many desirable optical and electronic properties, are commonly used in the semiconductor industry. The potential offered by integrating photonic band-gap structures with semiconductor devices could revolutionize optoelectronics and optical computing. It will be straightforward to extend our methods to metallic materials, which can readily be electrodeposited, and these three-dimensionally microperiodic metallic structures could well have unusual mechanical or thermal properties.

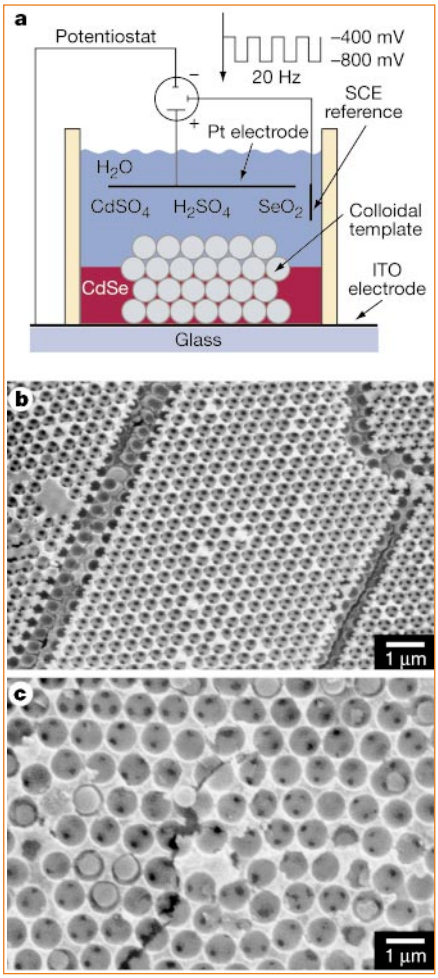

Figure 1 Electrodeposition in colloidal assemblies. **a,** Schematic representation of the experimental set-up. **b, c,** Scanning electron micrographs of the product. **b,** CdSe potentiostatically deposited in the interstitial space of a polystyrene colloidal assembly formed from polystyrene spheres 0.466 μm in diameter. After the electrodeposition, the polystyrene template was fully dissolved with toluene. SCE, standard calomel electrode; ITO, indium tin oxide. **c,** CdS galvanostatically grown around a silica colloidal template formed from silica spheres 1 μm in diameter. The template was partly dissolved after electrodeposition by dipping the sample into an aqueous 4.8% hydrogen fluoride solution for 10 min. This did not completely dissolve the template, allowing the relation between the colloidal template and the resulting three-dimensional structure to be seen directly.

Paul V. Braun*, Pierre Wiltzius
Bell Laboratories, Lucent Technologies, 700 Mountain Avenue, Murray Hill, New Jersey 07974, USA
**Present address: Department of Materials Science and Engineering, 1304 West Green Street, Urbana, Illinois 61801, USA*
e-mail: p-braun@uiuc.edu

1. Joannopoulos, J. D., Meade, R. D. & Winn, J. N. *Photonic Crystals: Molding the Flow of Light* (Princeton Univ. Press, New Jersey, 1995).
2. Holland, B. T., Blanford, C. F. & Stein, A. *Science* **281,** 538–540 (1998).
3. Wijnhoven, J. E. G. J. & Vos, W. L. *Science* **281,** 802–804 (1998).
4. Zakhidov, A. A. *et al. Science* **282,** 897–901 (1998).
5. Vlasov, Y. A., Yao, N. & Norris, D. J. *Adv. Mater.* **11,** 165–169 (1999).
6. Biswas, R., Sigalas, M. M., Subramania, G. & Ho, K.-M. *Phys. Rev. B* **57,** 3701–3705 (1998).
7. Busch, K. & John, S. *Phys. Rev. E* **58,** 3896–3908 (1998).
8. Lin, S. Y. *et al. Nature* **394,** 251–253 (1998).
9. Fleming, J. G. & Lin, S. Y. *Opt. Lett.* **24,** 49–51 (1999).
10. Imhof, A. & Pine, D. J. *Nature* **389,** 948–951 (1997).
11. Klein, J. D. *et al. Chem. Mater.* **5,** 902–904 (1993).
12. Edamura, T. & Muto, J. *Thin Solid Films* **235,** 198–201 (1993).

addendum

Colour categories in a stone-age tribe

J. Davidoff, I. Davies, D. Roberson
Nature **398,** 203–204 (1999)

The colour-naming pattern of Berinmo speakers may appear consistent with that obtaining in tritanopia[1], a colour-vision disorder that has an increased frequency in other tropical areas[2] and can arise from chronic exposure to short-wavelength light[3]. Furthermore, it could be argued that an isolated tribe may have become tritanopic through a shared genetic defect. However, our Berinmo speakers were not tritanopic. They were tested with the City University Colour Vision Test[4] that specifically assesses tritanopia. The test consists of ten plates, and all speakers who failed any of the plates were eliminated from our study. The failure rate was 7 out of 83 speakers tested during the course of the study.

1. Pokorny, J., Smith, V. C., Verriest, G. & Pinckers, A. J. L. G. *Congenital and Acquired Color Vision Defects* (Grune & Stratton, New York, 1979).
2. Davies, I. R. L., Laws, G., Corbett, G. G. & Jerrett, D. J. *Pers. Ind. Diff.* **25,** 1153–1162 (1998).
3. Werner, J. S., Peterzell, D. H. & Scheetz, A. J. *Optom. Vis. Sci.* **67,** 214–229 (1990).
4. Fletcher, R. *The City University Colour Vision Test* 2nd edn (Keeler, London, 1980).

corrections

Magnet levitation at your fingertips

A. K. Geim, M. D. Simon
Nature **400,** 323 (1999)

We inadvertently omitted a second reference to the work of I. A. H. Boerdijk (*Philips Res. Rep.* **11,** 45–56; 1956), where the first demonstration, to our knowledge, of levitation of a magnet using non-superconducting diamagnetic materials as stabilizers was reported. The more stable two-sided configuration was first described by Ponisovskii (*Prib. Tekh. Eksp.* **24,** 7–14; 1981). We were unaware of the earlier work until our experiments were completed.

Tropical tree gene flow and seed dispersal

M. B. Hamilton
Nature **401,** 129–130 (1999)

Two numbers were transposed in the last column of Table 1: for site 7, the values for populations 41-2 and 3209 should have been 1.0 and 0.0, respectively.

Tropical tree gene flow and seed dispersal

Deforestation affects the genetic structure of the surviving forest fragments.

In tropical forests, trees provide habitats and environmental conditions that support thousands of species. However, deforestation creates a mosaic landscape of cleared areas and forest fragments, which become the source of future tree populations. Fragmentation changes the movement of pollen and seed dispersal, modifying the gene flow and altering historical patterns of genetic subdivision. Paternity studies in tropical figs[1] and trees[2] have shown that pollen is dispersed over long distances, maintaining gene flow among widely spaced forest fragments, but gene movement by seed dispersal has not been studied in tropical trees. I have estimated chloroplast genome subdivision in the Amazonian canopy tree *Corythophora alta*, and here I show that seed dispersal is limited, with forest fragments as large as ten hectares being founded by a single maternal lineage.

Because trees are generally long-lived, the population-genetic effects of forest fragmentation are difficult to observe directly. Studies of gene flow provide an indirect means of gauging these effects and comparing the genetic structure in intact and fragmented forest. We can use the dispersal distances of pollen and seeds to estimate the size of a genetic 'neighbourhood' or the breeding area of a population. Paternal genes disperse through both pollen and seed, whereas maternal genes disperse only through seed. Total gene dispersal $\sigma^2 = (\sigma_p^2/2) + \sigma_s^2$, where σ_p^2 and σ_s^2 are the variances in pollen and seed movement, respectively, and the factor of 1/2 is required because pollen is haploid and we should omit the contribution of maternal gametes which do not disperse[3]. Seed-dispersal variance therefore contributes twice as much as pollen-dispersal variance to the size of genetic neighbourhoods.

Tissues were sampled from 162 mature trees (of at least 10 cm diameter at breast height) in four forest fragments and three sites of continuous forest at the Biological Dynamics of Forest Fragments Project near Manaus, Brazil (Fig. 1). The forest fragments were created in the early 1980s but mature trees established before forest clearance, as judged from growth rates for tree species of the family Lecythidaceae[4]. The sites are located within relatively homogeneous forest and are not separated by physical or ecological barriers to seed dispersal.

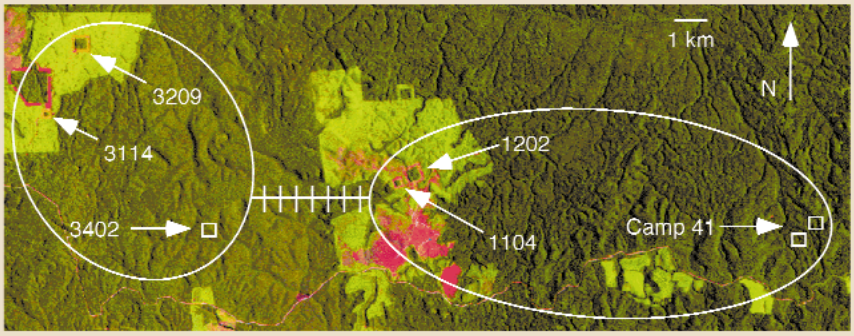

Figure 1 A 1995 LandSat image of the *C. alta* populations showing patterns of chloroplast (cp) DNA variation. Squares indicate continuous forest populations. Ellipses group populations with identical cpDNA haplotypes and the connecting line indicates seven haplotype differences between groups. Two trees with unique psbB-psbF haplotypes in population 3402 are not shown. Dark green, continuous forest; light green, second growth; pink, pasture.

Chloroplast (cp) DNA is maternally inherited in most angiosperms[5] and disperses only through seeds, so the spatial scale of cpDNA genetic differences among populations is a direct estimate of previous seed dispersal that led to trees being established[6]. Insertion or deletion polymorphisms were identified by sequencing five cpDNA regions[7,8]. Individual cpDNA haplotypes for seven polymorphisms were determined by allele-specific polymerase chain reaction (PCR). DNA sequence from random individuals verified that those with identical PCR haplotypes have identical cpDNA sequences. Haplotype frequencies among forest sites (Table 1) indicate almost complete cpDNA subdivision (the fixation index among populations, $F_{ST} = 0.992 \pm 0.042$; calculated according to ref. 9) among forest sites less than 10 km apart (Fig. 1). Forest fragments of 1 and 10 hectares all contain trees with a single cpDNA haplotype, indicating that they had a single maternal founder.

The pattern of cpDNA subdivision is consistent with historical seed dispersal being limited to small areas of continuous tropical forest. However, the seven populations are resolved into only two haplotype groups, so the extent of a seed-dispersal neighbourhood has not been estimated. Furthermore, selection can increase population subdivision in non-recombining organelle genomes[10], although there are no obvious differences in forest composition over this small spatial scale that could produce localized selection for cpDNA variants. I am now collecting data from adjacent populations and testing whether evolution in the chloroplast genome is consistent with a neutral model of substitution.

My results show that restricted seed-mediated gene flow has led to sharp genetic differentiation of adjacent populations. They indicate that small forest plots may exchange seeds infrequently, limiting the size of genetic neighbourhoods. Studies of gene flow in tropical trees have focused mostly on pollen dispersal, rather than seed dispersal, which may be more limited than pollen dispersal and is as likely to be altered by forest disturbance. Because gene flow through seeds is responsible for two-thirds of the total genetic-neighbourhood size, it is essential for estimates of the size of tropical-tree breeding populations. Gene flow from both seed and pollen dispersal will be required to predict fragmentation-induced genetic changes in tropical forest trees.

Table 1 Frequency of chloroplast genome insertion haplotypes for *C. alta*

			cpDNA site						
Population	Size (ha)	Number	1	2	3	4	5	6	7
1202	10	61	1.0	1.0	0.0	1.0	0.0	0.0	1.0
1104	1	1	1.0	1.0	0.0	1.0	0.0	0.0	1.0
41-1	10	16	1.0	1.0	0.0	1.0	0.0	0.0	1.0
41-2	10	20	1.0	1.0	0.0	1.0	0.0	0.0	0.0
3209	10	27	0.0	0.0	1.0	0.0	1.0	1.0	1.0
3114	1	8	0.0	0.0	1.0	0.0	1.0	1.0	0.0
3402	10	29	0.0	0.0	1.0	0.07	1.0	1.0	0.0

The cpDNA sites are: 1, trnL intron; 2, trnH-psbA 1; 3, trnH-psbA 2; 4, psbB-psbF; 5, rpl20-5' rps12; 6, trnS-trnG 172; and 7, trnS-trnG 520. Primers are described in ref. 8 for site 1 and in ref. 7 for all other sites.

Matthew B. Hamilton
Georgetown University, Department of Biology, Reiss Sciences 406, Washington DC 20057, USA and Biological Dynamics of Forest Fragments Project, National Institute for Research in the Amazon, CP 478, Manaus, AM 69011-970, Brazil
e-mail:hamiltmb@gusun.georgetown.edu

1. Chase, M. R., Moller, C., Kesseli, R. & Bawa, K. S. *Nature* **383,** 398–399 (1996).
2. Nason, J. D., Allen Herre, E. & Hamrick, J. L. *Nature* **391,** 685–687 (1998).
3. Crawford, T. J. *Heredity* **52,** 273–283 (1984).
4. Chambers, J. Q., Higuchi, N. & Schimel, J. P. *Nature* **391,** 135–136 (1998).
5. Reboud, X. & Zeyl, C. *Heredity* **72,** 132–140 (1994).
6. McCauley, D. E. *Trends Ecol .Evol.* **10,** 198–202 (1995).
7. Hamilton, M. B. *Mol. Ecol.* **8,** 521–522 (1999).
8. Taberlet, P. *et al. Plant Mol. Biol.* **17,** 1105–1109 (1991).
9. Weir, B. S. *Genetic Data Analysis II* (Sinauer, Sunderland, Massachusetts, 1996).
10. Rand, D. M. *Conserv. Biol.* **10,** 665–671 (1996).

Internet

Diameter of the World-Wide Web

Despite its increasing role in communication, the World-Wide Web remains uncontrolled: any individual or institution can create a website with any number of documents and links. This unregulated growth leads to a huge and complex web, which becomes a large directed graph whose vertices are documents and whose edges are links (URLs) that point from one document to another. The topology of this graph determines the web's connectivity and consequently how effectively we can locate information on it. But its enormous size (estimated to be at least 8×10^8 documents[1]) and the continual changing of documents and links make it impossible to catalogue all the vertices and edges.

The extent of the challenge in obtaining a complete topological map of the web is illustrated by the limitations of the commercial search engines: Northern Light, the search engine with the largest coverage, is estimated to index only 38% of the web[1]. Although much work has been done to map and characterize the Internet's infrastructure[2], little is known about what really matters in the search for information — the topology of the web. Here we take a step towards filling this gap: we have used local connectivity measurements to construct a topological model of the World-Wide Web, which has enabled us to explore and characterize its large-scale properties.

To determine the local connectivity of the web, we constructed a robot that adds to its database all URLs found on a document and recursively follows these to retrieve the related documents and URLs. We used the data collected to determine the probabilities $P_{out}(k)$ and $P_{in}(k)$ that a document has k outgoing and incoming links, respectively. We find that both $P_{out}(k)$ and $P_{in}(k)$ follow a power law over several orders of magnitude, remarkably different not only from the Poisson distribution predicted by the classical theory of random graphs[3,4], but also from the bounded distribution found in models of random networks[5].

The power-law tail indicates that the probability of finding documents with a large number of links is significant, as the network connectivity is dominated by highly connected web pages. Similarly, for incoming links, the probability of finding very popular addresses, to which a large number of other documents point, is non-negligible, an indication of the flocking nature of the web. Furthermore, while the owner of each web page has complete freedom in choosing the number of links on a document and the addresses to which they point, the overall system obeys scaling laws characteristic only of highly interactive self-organized systems and critical phenomena[6].

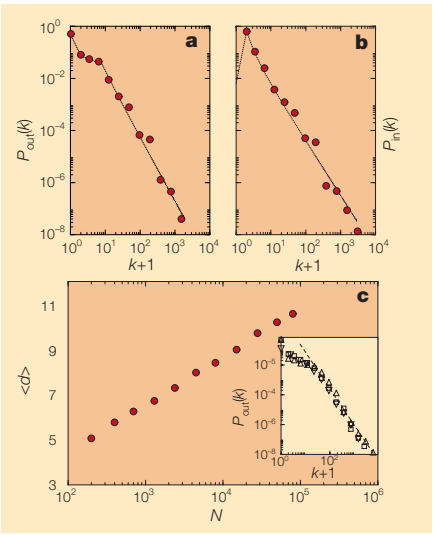

Figure 1 Distribution of links on the World-Wide Web. **a,** Outgoing links (URLs found on an HTML document); **b,** incoming links (URLs pointing to a certain HTML document). Data were obtained from the complete map of the nd.edu domain, which contains 325,729 documents and 1,469,680 links. Dotted lines represent analytical fits used as input distributions in constructing the topological model of the web; the tail of the distributions follows $P(k)\approx k^{-\gamma}$, with $\gamma_{out}=2.45$ and $\gamma_{in}=2.1$. **c,** Average of the shortest path between two documents as a function of system size, as predicted by the model. To check the validity of our predictions, we determined d for documents in the domain nd.edu. The measured $\langle d_{nd.edu}\rangle=11.2$ agrees well with the prediction $\langle d_{3\times10^5}\rangle=11.6$ obtained from our model. To show that the power-law tail of $P(k)$ is a universal feature of the web, the inset shows $P_{out}(k)$ obtained by starting from whitehouse.gov (squares), yahoo.com (triangles) and snu.ac.kr (inverted triangles). The slope of the dashed line is $\gamma_{out}=2.45$, as obtained from nd.edu in **a**.

To investigate the connectivity and the large-scale topological properties of the web, we constructed a directed random graph consisting of N vertices, assigning to each vertex k outgoing (or incoming) links, such that k is drawn from the power-law distribution of Fig. 1a,b. To achieve this, we randomly selected a vertex i and increased its outgoing (or incoming) connectivity to k_i+1 if the total number of vertices with k_i+1 outgoing (or incoming) links is less than $NP_{out}(k_i+1)$ (or $NP_{in}(k_i+1)$).

A particularly important quantity in a search process is the shortest path between two documents, d, defined as the smallest number of URL links that must be followed to navigate from one document to the other. We find that the average of d over all pairs of vertices is $\langle d\rangle=0.35+2.06\log(N)$ (Fig. 1c), indicating that the web forms a small-world network[5,7], which characterizes social or biological systems. For $N=8\times10^8$, $\langle d_{web}\rangle=18.59$; that is, two randomly chosen documents on the web are on average 19 clicks away from each other.

For a given N, d follows a gaussian distribution so $\langle d\rangle$ can be interpreted as the diameter of the web, a measure of the shortest distance between any two points in the system. Despite its huge size, our results indicate that the web is a highly connected graph with an average diameter of only 19 links. The logarithmic dependence of $\langle d\rangle$ on N is important to the future potential of the web: we find that the expected 1,000% increase in the size of the web over the next few years will change $\langle d\rangle$ very little, from 19 to only 21.

The relatively small value of $\langle d\rangle$ indicates that an intelligent agent, who can interpret the links and follow only the relevant one, can find the desired information quickly by navigating the web. But this is not the case for a robot that locates the information based on matching strings. We find that such a robot, aiming to identify a document at distance $\langle d\rangle$, needs to search $M(\langle d\rangle)\approx0.53\times N^{0.92}$ documents, which, with $N=8\times10^8$, leads to $M=8\times10^7$, or 10% of the whole web. This indicates that robots cannot benefit from the highly connected nature of the web, their only successful strategy being to index as much of the web as possible.

The scale-free nature of the link distributions indicates that collective phenomena play a previously unsuspected role in the development of the web[8], forcing us to look beyond the traditional random graph models[3–5,7]. A better understanding of the web's topology, aided by modelling efforts, is crucial in developing search algorithms or designing strategies for making information widely accessible on the World-Wide Web. Fortunately, the surprisingly small diameter of the web means that all that information is just a few clicks away.

Réka Albert, Hawoong Jeong, Albert-László Barabási
Department of Physics, University of Notre Dame, Notre Dame, Indiana 46556, USA
e-mail:alb@nd.edu

1. Lawrence, S. & Giles, C. L. *Nature* **400,** 107–109 (1999).
2. Claffy, K., Monk, T. E. & McRobb, D. Internet tomography. *Nature* [online] <http://helix.nature.com/webmatters/tomog/tomog.html> (1999).
3. Erdös, P. & Rényi, A. *Publ. Math. Inst. Hung. Acad. Sci.* **5,** 17–61 (1960).
4. Bollobás, B. *Random Graphs* (Academic, London, 1985).

Colour categories in a stone-age tribe

The Dani of Irian Jaya are a stone-age Melanesian people who have provided an empirical basis for the study of cross-cultural perception and cognition[1–3]. Although they had only two terms for describing colour, the Dani memory for colour seemed to be much like that of modern English speakers. We have investigated another stone-age culture, the Berinmo of Papua New Guinea, for the way in which they categorize colours, but the results do not support the idea that colour categories could be universal.

According to the linguistic relativity hypothesis[4,5], which is still influential, we construct our understanding of the world through language. Whorf[4] famously argued that, to an Eskimo, it would be unthinkable to use the same word for all types of snow because of its wide range of types and different uses.

We investigated colour in a remote, previously unstudied, hunter-gatherer tribe, the Berinmo, which lives on the upper reaches of the Sepik River in Papua New Guinea. When Berinmo subjects were asked to name the 160 colours in the standard Munsell array, thay used five basic colour terms[6]. The range and boundaries of these terms showed good intra-subject concordance, and can be seen in Fig.1 alongside the eight basic chromatic terms in English.

We replicated the Dani experiment with the Berinmo. The accuracy with which they remembered colours bore a striking similarity to the Dani; both groups of Melanesian subjects were very poor at this (9.6 and 7.7 out of 40, respectively). However, statistical analysis showed that, for both studies, the best statistical fit (that with the lowest stress value) was between Melanesian naming and Melanesian memory (Table 1a). This finding is consistent with the linguistic relativity hypothesis, but not with the interpretation of the original study.

The differences between English and Berinmo allow a further critical test of the contrast between colour universals and linguistic relativity. Berinmo does not mark the distinction between blue and green, but it has a colour boundary (between 'nol' and 'wor') in a position that does not exist in English. We investigated categorical effects[7,8] across both the blue–green and the nol–wor boundaries. We asked subjects to remember a colour over an interval of 30 seconds[1,2] and then select the same colour from a pair of similar alternatives. Sometimes the incorrect choice was from the same colour category and sometimes from a different one. We also added a 5-second-interval condition for the Berinmo as they had difficulty remembering blue–green samples for 30 seconds.

English subjects showed the expected advantage for cross-category blue–green decisions but not for nol–wor decisions; Berinmo subjects showed exactly the opposite pattern. The Berinmo showed no sign of a cross-category advantage for blue–green stimuli, but maintained their cross-category advantage for nol–wor stimuli both at 30 seconds and at 5 seconds. These results indicate that categorical perception occurs, but only for speakers of the language that marks the categorical distinction, which

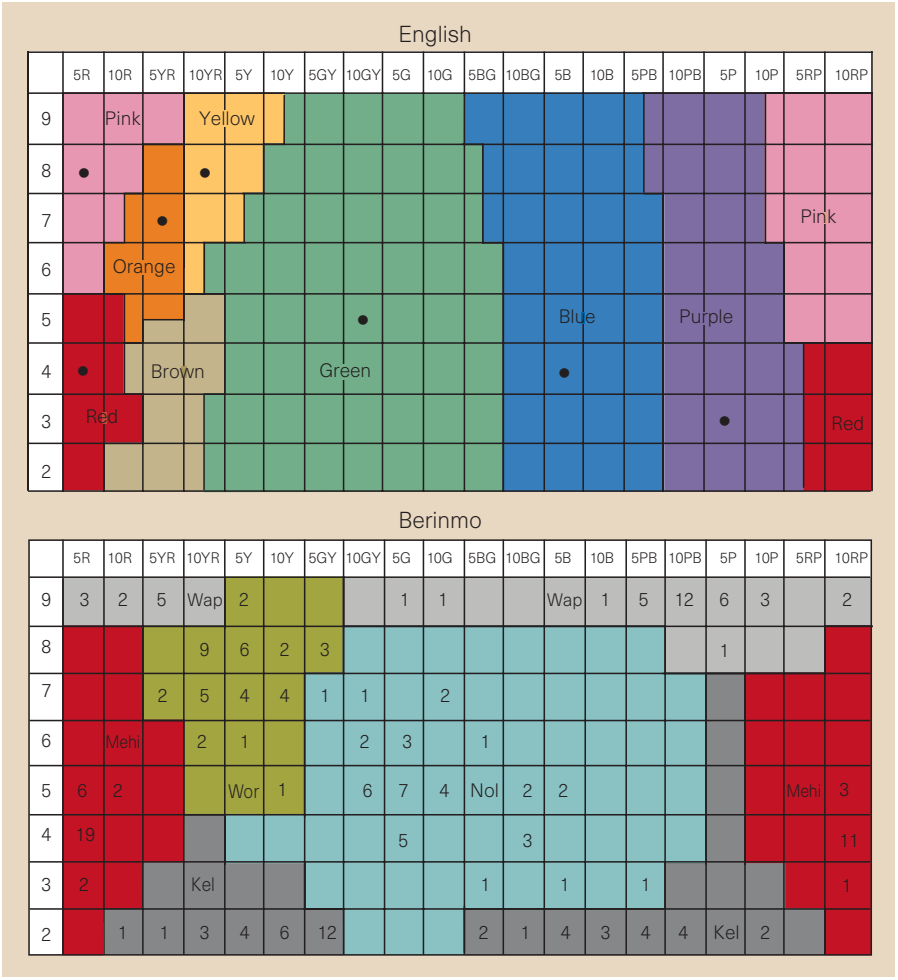

Figure 1 Distribution of English and Berinmo colour names. The Munsell system provides equally spaced samples in three dimensions, but is shown here as a Mercator projection of hue (horizontal axis) against lightness (vertical axis). The colours used to denote colour categories on these Mercator projections are for illustration only. Eight colour terms for English and five for Berinmo are shown. Dots on English naming data represent the position of focal colours[2]. Numbers on the Berinmo naming data represent the number of subjects who designated that colour as best example of the category. R, red; Y, yellow; G, green; B, blue; P, pink.

Table 1 **Statistical analysis of language data**

a Goodness of fit for multidimensional scaling solutions

Dani naming	versus	Dani memory	0.126
Dani memory	versus	US memory	0.161
Berinmo naming	versus	Berinmo memory	0.158
Berinmo memory	versus	English memory	0.256

b Mean trials to criteria in colour-categorization tasks

	Blue vs green	Green1 vs green 2	Nol vs wor	Yellow vs green
English speakers	3.2	5.9	3.8	1.4
Berinmo speakers	11.43	10.57	2.2	3.6

a, Measures of stress (departure from goodness of fit) are shown for comparison of naming and memory data. Low values indicate high goodness of fit. Data for comparisons between US naming and US memory are from ref. 1 and are compared with those from Berinmo and English subjects. In both cases, the fit between naming and memory is better than the fit between memory across language groups. b, Mean number of blocks to error-free performance. Categorizations are achieved more rapidly if they are consonant with distinctions made in the language of the subject.

is consistent with the linguistic relativity hypothesis.

If categories always form around natural fault lines in perceptual colour space, it should be relatively easy to learn another language's colour categories. To test this version of the universalist position, we asked English speakers to learn the nol–wor distinction and Berinmo speakers to learn the blue–green and yellow–green distinctions. For comparison, subjects were also asked to categorize stimuli in a manner consonant with the colour names of their own language. In addition, subjects learned a distinction not marked in either language: that between two types of green ('green 1' and 'green 2'). All tasks were made non-trivial by presenting only one stimulus at a time and by the inclusion of marginal examples of each category.

Berinmo subjects found learning to divide colours into green 1 and green 2 no harder than dividing them into blue and green; English speakers found the blue–green task easier. Berinmo subjects found the nol–wor task easier than the yellow–green task, whereas English subjects found the reverse. Tasks in which subjects divided stimuli varying in hue, lightness and saturation into two colour categories are performed better if the division corresponds to a linguistic, rather than a supposed universal, distinction (Table 1b).

Our results from these experiments are consistent with there being a considerable degree of linguistic influence on colour categorization, and place constraints on the type of neuron likely to underpin it. Neurons have been discovered in monkeys that are highly selective to wavelength[9], to combinations of wavelength and brightness[10] and to colour constancy[9], but it is unlikely that there are neurons that respond to all examples of a colour category unless their operation is susceptible to linguistic modification.

Jules Davidoff*, Ian Davies†, Debi Roberson*

**Goldsmiths' College, University of London, London SE14 6NW, UK*
e-mail: j.davidoff@gold.ac.uk
†Department of Psychology, University of Surrey, Guildford, Surrey GU2 5XH, UK

1. Heider, E. R. & Olivier, D. C. *Cogn. Psychol.* **3,** 337–354 (1972).
2. Heider, E. R. *J. Exp. Psychol.* **93,** 10–20 (1972).
3. Hardin, C. L. & Maffi, L. in *Color Categories in Thought and Language* (eds Hardin, C. L. & Maffi, L.) 1–18, 347–372 (Cambridge Univ. Press, 1997).
4. Whorf, B. *Language, Thought and Reality* (MIT Press, Cambridge, Massachusetts, 1956).
5. Saunders, B. A. C. & van Brakel, J. *Behav. Brain Sci.* **20,** 167–228 (1997).
6. Berlin, B. & Kay, P. *Basic Color Terms: Their Universality and Evolution* (Univ. California Press, Berkeley, 1969).
7. Bornstein, M. H. & Korda, N. O. *Psychol. Res.* **46,** 207–222 (1984).
8. Calder, A. J., Young, A. W., Perrett, D. I., Etcoff, N. L. & Rowland, D. *Vis. Cogn.* **3,** 81–117 (1996).
9. Zeki, S. *Neuroscience* **9,** 741–765 (1983).
10. Yoshioka, T., Dow, B. M. & Vautin, R. G. *Behav. Brain Res.* **76,** 51–70 (1996).

Why biodiversity surveys are good value

Article 8 of the Convention on Biological Diversity obliges contracting parties to establish protected areas for conservation. This can be achieved in smaller networks of reserves if their design is based on how well different sites complement one another biologically, rather than on more commonly used criteria, such as species richness or simple availability for acquisition[1,2]. However, this increase in efficiency[3] requires species lists for each candidate site, and obtaining such data can be expensive; for example, a detailed survey of five taxa across 15,000 km^2 of forest in Uganda took nearly 100 person-years and cost about US$1 million[4,5]. Here we ask whether investing in such surveys makes economic sense, or whether conservation agencies would be better advised to continue following more traditional reserve selection procedures, at the cost of having to conserve larger reserve networks.

This trade-off is shown in Fig. 1. Using a simple reserve selection rule (such as buying relatively intact land as it becomes available[1]) results in an inefficient reserve network, whose cumulative representation of biodiversity rises only slowly with increasing area. But if a complementarity-based algorithm is used instead, the network needed to achieve a particular conservation goal is reduced by an area a. The greater cost of conserving the less efficient network has a present value equal to $[a(x+y/r)]$, where x is the mean purchase cost of a unit area of land for conservation, and y is the mean cost per unit area of effective maintenance, discounted into the future at an annual rate r. In contrast, conducting a high-quality survey costs zA, where A is the total area of all the candidate sites surveyed, and z is the survey cost per unit area. It follows that investing in surveys is good value provided that $zA < [a(x+y/r)]$ or alternatively that $z < [(a/A)(x+y/r)]$. This therefore sets the upper limit of cost-effective surveys for reserve selection.

There are few published data with which to parametrize this simple model. Conservatively, we suggest that a/A (the relative saving in reserve area achieved by tackling complementarity) is commonly at least 5%; it will often be far higher[1]. Estimates for x and y, obtained from a diverse range of sources and expressed in 1990 US$, are summarized in Table 1. Using appropriate values for r (from 5% to 20%), we can then estimate $[(a/A)(x+y/r)]$. Marked variation in land prices[6] and labour costs means that this upper limit of cost-effective surveys varies enormously but, wherever data are available, this greatly exceeds the likely cost of high-quality surveys. For instance, in Uganda, at $r = 10\%$, $[(a/A)(x+y/r)] \approx \$800$ per km^2, whereas the true value of z is less than one-tenth of this, at $58 per km^2. Reversing this calculation, detailed inventories would have to yield area savings of less than 0.4% — that is, $a/A < z/[x+y/r]$ — for them not to be worthwhile. This condition is extremely unlikely to be met[1]. So, in Uganda, detailed biodiversity inventories represent a very good conservation investment.

In other developing countries, the costs of detailed surveys for reserve selection are similar ($z \approx \$65$ per km^2 in Sri Lanka[7], and $z \approx \$135$ per km^2 in Yemen; A. Miller, personal communication), and far less than corresponding values for $[(a/A)(x+y/r)]$, which range from several hundred to a few thousand dollars per km^2 (Table 1). In developed countries, $[(a/A)(x+y/r)]$ is typically much higher (Table 1) and, although the labour costs of surveys are also high, these are generally offset by the greater availability of existing inventory data. As a result, in the United Kingdom, $z \approx \$1{,}500$ per km^2 (M. Drake and R. Porley, personal communication), which is much less than $[(a/A)(x+y/r)]$. In Australia, on average, $z \ll [(a/A)(x+y/r)]$, at just $5 per km^2 (ref. 8). As in some other countries, the Australian mean value masks huge local variation in all costs; nevertheless, in arid areas

Table 1 Estimates of the costs of buying and maintaining nature reserves

	Cost of land purchase, x ($ per km^2)	Cost of effective maintenance, y ($ per km^2)	Present value of maintenance, y/r ($ per km^2)			$(a/A)(x+y/r)$ (assuming $a/A = 5\%$)
			$r = 5\%$	$r = 10\%$	$r = 20\%$	($ per km^2)
Uganda	12,628	383	7,660	**3,830**	1,915	**823**
Ghana[12]	45,215	236	4,720	**2,360**	1,180	**2,379**
South Africa[13]	21,896	1,600	32,000	**16,000**	8,000	**1,895**
Brazil[12,14]	10,776	169	3,380	**1,690**	845	**623**
Belize[12,15]	14,087	350	7,000	**3,500**	1,750	**879**
UK	100,523	6,443	**128,860**	64,430	32,215	**11,469**
USA[12]	78,730	2,053	**41,060**	20,530	10,265	**5,990**
Australia[8,12]	385	359	**7,180**	3,590	1,795	**378**

Figures are in 1990 US$ and often mask considerable local variation. Figures in bold are based on $r \div 10\%$ for developing countries and $r \div 5\%$ for developed countries, but our conclusions are robust for $5\% < r < 20\%$. Data were generously provided by T. Butynski, P. Howard, the African Wildlife Foundation, Conservation International, Fauna and Flora International, Kwa Zulu Natal Nature Conservation Service, Royal Society for the Protection of Birds, the Nature Conservancy, and the Western Australia Department of Conservation and Land Management, and cited sources.

Magnet levitation at your fingertips

The stable levitation of magnets is forbidden by Earnshaw's theorem, which states that no stationary object made of magnets in a fixed configuration can be held in stable equilibrium by any combination of static magnetic or gravitational forces[1–3]. Earnshaw's theorem can be viewed as a consequence of the Maxwell equations, which do not allow the magnitude of a magnetic field in a free space to possess a maximum, as required for stable equilibrium. Diamagnets (which respond to magnetic fields with mild repulsion) are known to flout the theorem, as their negative susceptibility results in the requirement of a minimum rather than a maximum in the field's magnitude[2–4]. Nevertheless, levitation of a magnet without using superconductors is widely thought to be impossible. We find that the stable levitation of a magnet can be achieved using the feeble diamagnetism of materials that are normally perceived as being non-magnetic, so that even human fingers can keep a magnet hovering in mid-air without touching it.

Stable levitation has been demonstrated for diamagnetic objects such as superconducting pellets and live creatures[2,5–7]. Strong diamagnetism of superconductors allows the situation to be reversed, so that a magnet can be levitated above a superconductor[8]. Paramagnetic objects can also be levitated if placed in a stronger paramagnetic medium, such as ferrofluid or oxygen, which makes them effectively diamagnetic[9].

We set out to lift a magnet by applying a magnetic field and then stabilizing the intrinsically unstable equilibrium with repulsive forces from a nearby diamagnetic material. We found that, surprisingly, the forces created by almost non-magnetic materials (susceptibility χ of about 10^{-5}) are sufficient to stabilize levitation over distances as large as several millimetres under Earth gravity conditions, even though they decay rapidly with distance as $1/x^5$ (Fig. 1).

For stable levitation, an equilibrium requires that the magnetic force $MB'(z)$ compensates the gravitational force mg, where M is the magnetic moment and $B(z)$ and $B'(z)$ are the magnetic field on the axis and its derivative, respectively. For the equilibrium to be stable, it must be in a region where the total energy of the magnet $U = -\boldsymbol{MB}(\boldsymbol{r}) + mgz + U_{dia}$ has a minimum ($\Delta U > 0$), where U_{dia} is the energy of diamagnetic interaction with the cylinder. Close to the equilibrium position at the field axis[3,10],

$$U \approx U_0 + [mg - MB'(z)]z + K_v z^2 + K_h r^2 + Cr^2 + \ldots \quad (1)$$

where $K_v(z) \equiv -MB''(z)/2$ and $K_h(z) \equiv -M[B'(z)^2 - 2B(z)B''(z)]/8B(z)$.

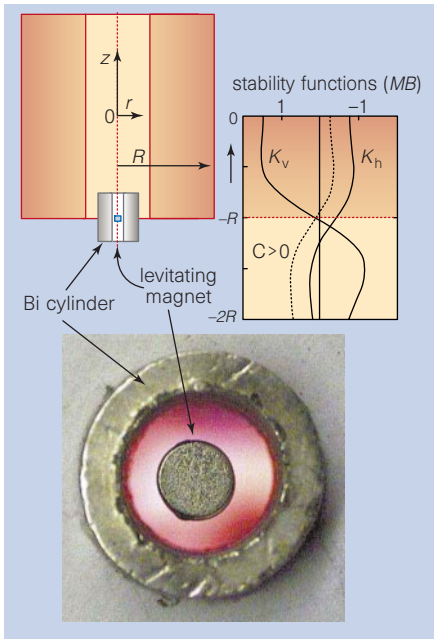

Figure 1 A NdFeB magnet (an alloy of neodymium, iron and boron; 4 mm high and 4 mm in diameter) levitating at the axis of a vertical solenoid of radius $R \approx 10$ cm and length $\approx 2R$ in a magnetic field of 100 gauss. The levitation is stabilized by a bismuth cylinder ($\chi = -1.5 \times 10^{-4}$) with inner diameter $D \approx 8$ mm. The photograph shows the top view of the levitating magnet. The right-hand plot shows the stability functions K_v and K_h calculated for a solenoid with a height of twice its radius (solid curves). Diamagnetic interaction C shifts the horizontal stability function K_h to the left (dashed curve) and a small region of positive ΔU emerges above the point where $K_v = 0$.

The presence of a diamagnetic cylinder results in the last term in equation (1) and, for the geometry of Fig. 1, we find that $C = 45\mu_0|\chi|M^2/16D^5$, where μ_0 is the permeability of free space. If there is no diamagnet ($C = 0$), the stability can never be reached (at no point are K_v and K_h both positive; Fig. 1). The diamagnetic interaction allows the energy U to have a minimum ($K_v > 0$ and $K_h + C > 0$) which emerges for $C > MB'(z)^2/8B(z)$ just above the point of a maximum field gradient ($B''(z) = 0$). It is counterintuitive that levitation is easiest in the most inhomogeneous field region, rather than in the centre of a solenoid where the field is almost uniform.

It is instructive to introduce a characteristic scale L on which the field changes: $B' = B/L$. At the optimum levitation point ($B''(z) = 0$), L varies between R and $1.2R$ for long and short solenoids, respectively. If we approximate our levitating magnet by a sphere of diameter d with a remnant field B_r, then $M = (\pi/4\mu_0)B_r d^3$, and the requirement for levitation becomes

$$A(|\chi|LB_r^2 d^3/\mu_0 \rho g)^{1/5} > D > d \quad (2)$$

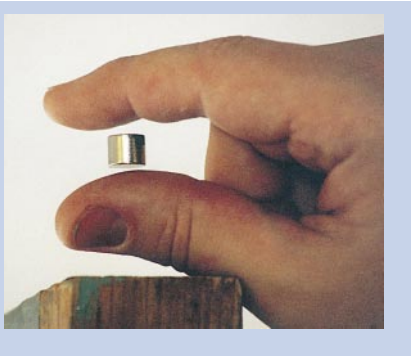

Figure 2 Levitation at your fingertips. A strong NdFeB magnet (1.4 tesla) levitates 2.5 metres below a powerful superconducting magnet. The field at the levitation point is about 500 Gauss.

where ρ is the density of the magnet's material and $A \approx 1.92$. Calculation shows that a magnet several millimetres in size with remnant magnetization of about 1 tesla (NdFeB) can be levitated with a clearance gap, $D - d$, of several millimetres using a 10-cm solenoid and strongly diamagnetic Bi or graphite, in agreement with our experiment.

Equation (2) depends on the product of χ and L, which means that by increasing L (scaling up the magnet's size) we can achieve the same D as above using ordinary materials (such as plastic or wood, with $\chi \approx -10^{-5}$). To illustrate this point, we show another example of a levitating magnet in Fig. 2 in which human fingers ($\chi \approx -10^{-5}$) are used as diamagnetic stabilizers. Here we use an alternative geometry[11] in which L is easier to scale up because it is determined not only by the magnet size, but also by its strength. The levitating magnet is placed below a solenoid in the region where the equilibrium is stable horizontally ($K_h > 0$) but not vertically ($K_v < 0$) (Fig. 1). Vertical stability is achieved by means of two horizontal diamagnetic plates (or by the fingertips).

In this geometry, the positive constant $C = 6\mu_0|\chi|M^2/\pi D^5$ counters K_v and the levitation condition is similar to equation (2), except that now D denotes the separation between the plates, $A \approx 1.02$ and $L \equiv 4B'/B''$ is approximately the distance from the centre of a solenoid to a levitating magnet. The larger the distance, the easier it is to stabilize levitation by diamagnetic repulsion. L is limited by the requirement on the field gradient, $B'(z) = mg/M$. To reach such a large L, as in Fig. 2, we used an 11-tesla superconducting solenoid a metre in diameter. If stronger diamagnets are used (such as graphite or bismuth), this type of levitation can also be achieved with small permanent magnets, making miniature hand-held

devices accessible to everyone (M. D. S., unpublished data). These could replace the existing servo levitation devices for some applications.

A. K. Geim*, M. D. Simon†, M. I. Boamfa*, L. O. Heflinger†

**High Field Magnet Laboratory, University of Nijmegen, 6525 ED Nijmegen, The Netherlands*
e-mail: geim@sci.kun.nl
†Department of Physics and Astronomy, University of California at Los Angeles, Los Angeles, California 90095, USA

1. Earnshaw, S. *Trans. Camb. Phil. Soc.* **7,** 97–112 (1842).
2. Brandt, E. H. *Science* **243,** 349–355 (1989).
3. Berry, M. V. & Geim, A. K. *Eur. J. Phys.* **18,** 307–313 (1997).
4. Thomson, W. (Lord Kelvin) *Reprints of Papers on Electrostatics and Magnetism* (Macmillan, London, 1872).
5. Braunbeck, W. *Z. Phys.* **112,** 753–763 (1939).
6. Beaugnon, E. & Tournier, R. *Nature* **349,** 470 (1991).
7. Geim, A. *Phys. Today* **51,** 36–39 (September 1998).
8. Arkadiev, A. *Nature* **160,** 330 (1947).
9. Ikezoe, Y. *et al. Nature* **393,** 749–750 (1998).
10. Simon, M. D. *et al. Am. J. Phys.* **65,** 286–292 (1997).
11. Boerdijk, A. H. *Philips Tech. Rev.* **18,** 125–127 (1956).

Extraocular magnetic compass in newts

Geomagnetic orientation is widespread among organisms, but the mechanism(s) of magnetoreception has not been identified convincingly in any animal[1]. In agreement with biophysical models proposing that the geomagnetic field interacts with photoreceptors[2–4], changes in the wavelength of light have been shown to influence magnetic compass orientation in an amphibian, an insect and several species of birds (reviewed in ref. 5). We find that light-dependent magnetic orientation in the eastern red-spotted newt, *Notophthalmus viridescens*, is mediated by extraocular photoreceptors, probably located in the pineal complex or deeper in the brain (perhaps the hypothalamus).

Experiments investigating shoreward magnetic compass orientation have demonstrated that the newt's perception of the direction of the magnetic field is rotated 90° under long-wavelength (greater than 500 nm) light[5,6]. We recently trained newts under natural skylight to aim for the shore by placing them for 12–16 hours in water-filled tanks with an artificial shore at one end[5,7]. The magnetic orientation of individual newts was then tested in a circular, visually symmetrical indoor arena under depolarized light. Under full-spectrum light (from a xenon arc source), they exhibited bimodal magnetic orientation parallel to the shoreward axis in the training tank (Fig. 1a,d). In contrast, under long-wavelength light, they orientated themselves perpendicular to the shoreward direction (Fig. 1b,e).

To demonstrate that the 90° shift in orientation under long-wavelength light was due to a direct effect of light on the newts' perception of the magnetic field, we trained newts under long-wavelength light by covering the training tank with a long-wavelength-transmitting gel filter (two layers of Lee #101)[5]. Under long-wavelength light, these newts orientated themselves parallel to the shoreward axis, indicating that they had learned the direction of the shore with respect to the rotated magnetic information under long-wavelength light (Fig. 1c,f).

As well as ocular photoreceptors, newts have extraocular photoreceptors in the pineal complex[8] and possibly the hypothalamus[9]. To determine which photoreceptors are involved in the magnetic compass response, we manipulated the wavelength of light reaching the extraocular photoreceptors. Small round 'caps' (5 mm in diameter) were attached to the dorsal surface of the head of each newt using cyanoacrylate glue, and remained in place during both training and testing. Equal numbers of newts were capped with either a clear filter (Lee #130) or a filter that transmitted only long-wavelength light (equivalent to two layers of Lee #101). The caps were positioned to alter the spectral properties of light reaching the pineal and surrounding structures, whereas light reaching the eyes was unaffected. Clear-capped newts were tested to control for any nonspecific effects of the caps on the newts' orientation behaviour.

All newts were trained outdoors under natural skylight and tested for magnetic orientation in the testing arena under long-

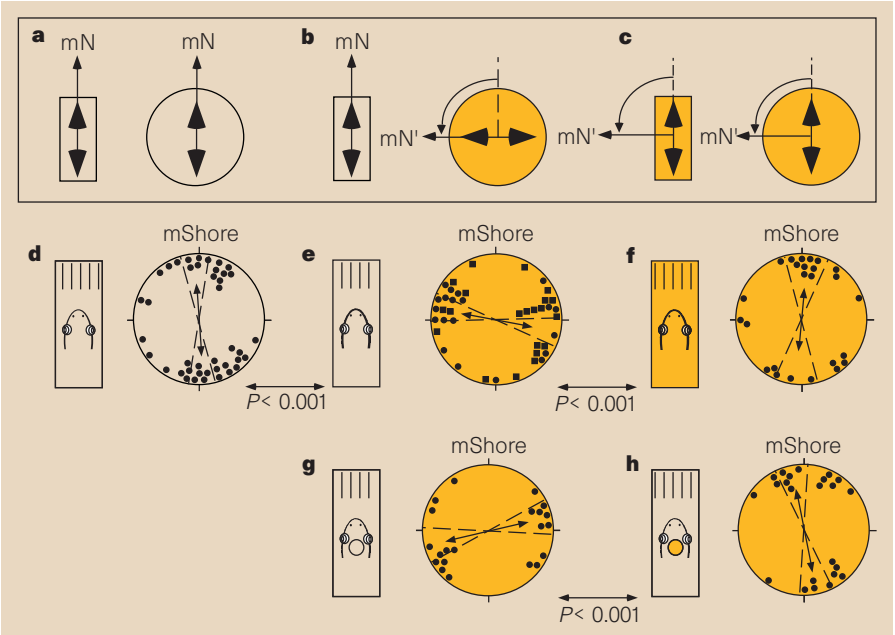

Figure 1 Effects of long-wavelength light and head caps on bimodal magnetic orientation in newts. **a–c,** Predicted orientation of newts (double-headed arrow) and their perception of the direction of the magnetic field (single-headed arrow)[5,6]. Training tanks have the shore towards magnetic north (mN); circular test arenas show the predicted response of the newts under either full-spectrum (beige) or long-wavelength light (yellow). **a,** Full-spectrum training and testing: newts should perceive the shore to be towards magnetic north and exhibit bimodal magnetic orientation along the shoreward axis. **b,** Full-spectrum training, long-wavelength testing: newts' perception of magnetic north in testing, and their orientation in the test arena, should be rotated 90° (mN′) from magnetic north during training. **c,** Long-wavelength training and testing: newts' perception of the magnetic field should be rotated 90° relative to the actual field during training and testing. Their perception of the magnetic field in the arena would be the same as in the outdoor tank. **d–h,** Results. Data points show the magnetic bearing of a newt tested in one of four symmetrical alignments of an Earth-strength magnetic field (magnetic north is geographic north (gN), east (gE), west (gW) or south (gS)). The magnetic field was altered by two orthogonally orientated, double-wrapped, Ruben's coils around the test arena[7]. Data are plotted with respect to the magnetic direction of shore (mShore) in the training tank (shore direction, 360°). Double-headed arrows indicate mean axis of orientation with the mean axis length, r, proportional to the strength of orientation (diameter of the circle corresponding to $r=1$). Dashed lines indicate 95% confidence intervals for the mean axis. Distributions are significant at $P<0.05$ or less by the Rayleigh test and P-values between circle plots indicate significant differences between distributions (Watson U^2 test). **d,** Newts trained under natural light and tested under full-spectrum light orientated along the shoreward axis[5]. **e,** Newts trained under natural light and tested under long-wavelength light orientated 90° from the shoreward direction (filled circles; tested under broadband long-wavelength (≥500 nm) light; filled squares, tested under a 550-nm light, 40 nm bandwidth, 12.5 ± 0.1 log Quanta cm^{-2} s^{-1}; ref. 5). **f,** Newts trained and tested under long-wavelength light orientated along the shoreward axis[5]. **g,** After training under natural light, clear-capped newts tested under long-wavelength light orientated ~90° from the shoreward direction. **h,** After training under natural light, newts with long-wavelength-transmitting caps orientated along the shoreward axis under long-wavelength light.